Published in: Chemical Physics (1992) vol. 160, pp. 477-485.
Status: Postprint (Author's Version)

Photoionization mass spectrometry of kinetic energy-selected ions. The translational energy distribution of N^+/N_2 in the inner-shell ionization energy range

R. Locht

Département de Chimie Générale et de Chimie Physique, Institut de Chimie, Bât. B6, Université de Liège, Sart-Tilman par B-4000 Liège 1, Belgium

W. Denzer, E. Rühl and H. Baumgärtel

Institut für Physikalische und Theoretische Chemie, Freie Universität Berlin, Takustrasse 3, W-1000 Berlin 33, Germany

Abstract

An ion retarding potential difference (IRPD) method has been used to investigate the ion yield and kinetic energy distributions of N^+/N_2 produced by photoionization mass spectrometry using synchrotron radiation. Photoion yield curves of energy selected N^+ ions are deduced. Translational energy distributions of N^+ at energies of the N(1s)→π*, N(1s)→ $(nl)^1$ and above the $N(1s)^{-1}$ threshold are determined. Comparison is made with previous photoion-photoelectron coincidence work using time-of-flight (TOF) measurements.

1. Introduction

The soft X-ray absorption by a molecule promotes a core electron to an unoccupied valence molecular and Rydberg orbital or into the continuum. This leads to a cascade of events which mostly ends up in the dissociation of the molecule. The initial excitation is followed by an Auger-type transition depleting bonding orbitals and eventually populating antibonding orbitals. Consequently the molecule falls apart into singly- and multiply charged fragments and/or neutrals. Singly charged fragments are formed either by single ionization or by dissociative double ionization. The products of the latter process are usually characterized by an extended translational energy distribution because of electrostatic repulsion ("Coulomb explosion"). The investigation of these phenomena in the gas phase are important to help to understand fragmentation processes occurring in the energy range of valence- and Rydberg orbitals excitation and above the inner-shell ionization. Recently, Hanson [1] published an updated review on this particular subject.

The inner-shell dissociative photoionization of N_2 has been investigated by mainly two groups, using synchrotron radiation as a soft X-ray source.

Eberhardt et al. [2] investigated simultaneous electron emission and fragment ion production from N_2 by core level excitation. Undissociated parent cations (N_2^+) were related to N(1s)→π* excitation, whereas the formation of N^{2+} fragments was related to a hole in the $2\sigma_u$ orbital.

The same authors [3] performed Auger electron-ion coincidence experiments. They were able to correlate fragment ions, their translational energy and their electronic configuration with the hole configuration of the doubly charged molecular ion.

Saito and Suzuki [4,5] investigated the same system by means of a time-of-flight (TOF) mass spectrometric technique. The TOF-spectra resulting from the N(1s)→π* excitation and the $N(1s)^{-1}$ ionization are different. Kinetic energy distributions and angular distributions [6,7] were determined. By photoion-photoion coincidence $N^+ + N^+$ and $N^{2+} + N^+$ dissociations were characterized [6]. The N_2 fragmentation after $N(1s)^{-1} \rightarrow (nl)^1$ excitation has been examined separately [8].

In all these papers discrete values of the kinetic energy of the fragment ions are derived from TOF-simulation calculations. The sum of these contributions is compared to the observed TOF-distributions.

To study dissociative photoionization processes, a new method has recently been proposed [9]. It is mainly based on (i) fragment ions translational energy distribution measurements by means of a retarding potential method and (ii) ionization efficiency curves measurements for preset retarding potential settings. It has

been tested for NO^+ and O^+ formation from N_2O in the valence-shell ionization energy range. This method has been shown to be well suited for the investigation of resonant dissociative ionization processes, e.g. autoionization.

The aim of this paper is to apply the abovementioned method to the dissociative ionization of N_2 in the core-excitation and ionization energy region. A further motivation for such gas phase photodissociative ionization studies in this energy range is to obtain useful data for photon stimulated ion desorption (PSID) investigations. Notwithstanding observed differences (e.g. between PSID and electron energy-loss spectra (EELS)), Rosenberg et al. [10] evinced many similarities between gas phase and solid phase investigations of the same molecular systems. The retarding potential technique being often used in this field, the presently described method could adequately been applied.

2. Experimental

The experimental setup used in this photoionization work has been described elsewhere [9,11] and only the most salient features will be repeated here.

The ions produced by photoionization are extracted by a weak drawout field of about 120 mV/cm and focussed on the exit hole of the ion source. The emerging ion beam is energy-analyzed in a retarding lens and accelerated in a quadrupole mass filter. The ion counting pulse from a channeltron multiplier, is continuously scanned as a function of the wavelength λ at fixed retarding potential V_R (ion yield curves) or of the retarding potential V_R at fixed photon wavelength λ (retarding potential curves). The first derivative of the retarding potential curve, or the kinetic energy distribution, is obtained numerically.

The maximum of the N_2^+ ion translational energy distribution is used as zero-energy calibration point of the N^+ ions kinetic energy scale. The same reference is used during the recording of the photoionization efficiency curves of N^+ at different retarding potential settings. The energy resolution of the kinetic energy-analyzer in the present experimental conditions is 100 meV as measured on the fwhm of the N_2^+ kinetic energy distribution.

The main differing feature in the present experiment is the use of a high energy toroidal grating monochromator HE-TGM-2 to disperse the light continuum from the synchrotron radiation of the Berlin electron storage ring BESSY. This monochromator has been described elsewhere [12].

A 1500 l/mm grating is used throughout this work. Entrance and exit slits of 200 μm are used for ion yield measurements without retarding field. A resolution of about 0.5 eV is obtained, as measured on the N(1s)→π* resonance. In order to gain ion signal intensity when a retarding potential is applied to the ion beam, both entrance and exit slits are opened to 400 μm.

The N_2-gas sample (Messer Griesheim, purity 99.999%) is introduced in the ion chamber at a pressure of 10^{-5}mbar.

3. Results, data acquisition and handling

The photoionization mass spectrum of N_2 is measured at λ =3.095 nm (400.60 eV) when a -0.5 V negative voltage is applied to the retarding grid. The intensity ratios $N_2^+/N^+/N^{2+}$ are about 0.72/0.26/ 0.02.

The photoionization efficiency curves of N^+ are recorded between 2.9 nm (417 eV)$<\lambda<$3.2 nm (387.4 eV) and for retarding potential settings ranging -0.5$<V_R<$8.0 V by 0.5 V steps. The N^+ and N_2^+ ion yield curves recorded at V_R = -0.5 V are normalized with respect to the mass spectrum recorded at λ=3.095 nm (400.6 eV).

N^+ photoion retarding potential curves have been recorded at λ=3.095 nm (400.6 eV) and λ=2.959 nm (419.0 eV). Both retarding potential curves are intensity normalized to the ionization efficiency at both wavelengths and for V_R = - 0.5 V. These curves are shown in fig. 1, the intensities being on an arbitrary scale. The intensity ratio $i(N^+)_{3.095}/i(N^+)_{2.959}$ at different corrected retarding potential settings are listed in table 1.

Finally the photoionization efficiency curves of N^+ recorded for retarding potential settings ranging from -0.5 V$<V_R<$8.0 V are normalized to the normalized retarding curve at λ.=2.959 nm (419 eV). The intensity ratios $i(N^+)_{3.095nm}/i(N^+)_{2.959nm}$ measured for different retarding potential settings are listed in the third column of table 1. The ratios obtained in both ways are consistent within experimental error. The photoion yield curves

Published in: Chemical Physics (1992) vol. 160, pp. 477-485.
Status: Postprint (Author's Version)

handled in this way are gathered in fig. 2 between $0.4<V_R<1.9$ V. The N^+ ion retarding curve measured at λ=2.959 nm (419 eV) is also inserted in this figure.

***Fig. 1**. Photoion retarding potential curves of N^+/N_2 recorded at λ=3.095 nm (400.6 eV) and at λ=2.959 nm (419 eV).*

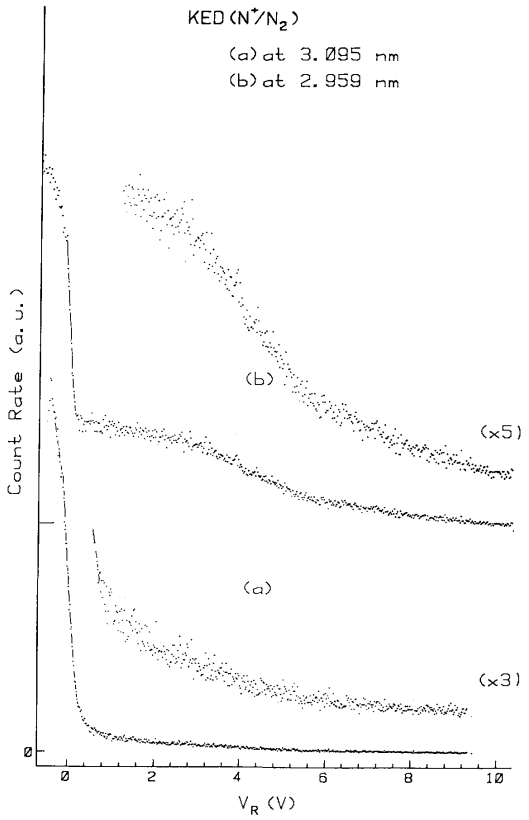

***Table 1.** Comparison of the ratio $R=i(N^+)_{3.09nm}/i(N^+)_{2.96nm}$ measured for N^+ photoion retarding curves recorded at both wavelengths (R_{KED}) and for N^+ photoion yield curves at different V_R settings (R_{PIC}) [a)]*

V_R(V)	R_{KED}	R_{PIC}
0.38	0.85 ±0.10	0.96 ±0.10
0.88	0.46 ±0.09	0.44 ±0.09
1.38	0.38 ±0.09	0.25 ±0.06
1.88	0.29 ±0.06	0.22 ±0.05
2.38	0.27 ±0.06	0.22 ±0.05
2.88	0.26 ±0.06	0.19 ±0.05
3.38	0.23 ±0.06	0.19 ±0.05
4.38	0.21 ±0.06	0.16 ±0.06
5.38	0.21 ±0.15	0.19 ±0.1
7.90	0.15 ±0.15	0.12 ±0.1

[a)] At V_R=-0.5 V, $i(N^+)_{3.095nm}/i(N^+)_{2.959nm}$ = 9.6.

By subtracting the normalized photoion yield curves obtained at the successive retarding potential settings, ion retarding potential difference (IRPD) curves are obtained. These are displayed in fig. 3. The intensity distribution at fixed wavelength is directly related to the kinetic energy distribution.

In order to estimate the importance of the discrimination of N^+ fragment ions with different initial translational energies, the present retarding field analyzer [13] has been compared with a 90°-condenser analyzer

[14] and a time-of-flight (TOF) [15]. The present experimental setup being identical to that described earlier [13] this comparison is made in the valence ionization energy region for N^+/N_2 and for a kinetic energy distribution spreading from 0-8 eV measured at 90° with respect to the ionizing electron beam. For $0<KE(N^+)<5$ eV ions agreement is found within 5%. However, the TOF-experiment shows drastic discrepancies below 2 eV kinetic energy. The thermal component of the distribution is not observed. For $5<KE(N^+)<8$ eV the TOF-experiment [15] shows less energetic N^+ ions (≈ 10%) whereas the deflection analyzer [14] shows more high-energy N^+ ions (20-50%).

4. Discussion

4.1. The excitation spectrum of N_2

The excitation spectrum of N_2 in the inner-shell ionization region has abundantly been investigated by low- and high-energy resolution electron energy-loss spectroscopy [16-19]. Photoabsorption spectra of relatively low resolution (0.5 eV) were measured using synchrotron radiation [20,21]. Recently, higher resolution (0.15 eV) photoabsorption spectra were obtained under the same conditions using a plane grating monochromator SX-700 at BESSY (Berlin) [22,23].

Below the N(1s) ionization energy, the absorption and electron energy-loss spectra of N_2 show several resonances assigned to $N(1s)\rightarrow 2p\pi_g(\pi^*)$ transition and to Rydberg excitations $N(1s)\rightarrow n(s, p, d)$ and n(p,d) [16-19]. Above the K-shell ionization limit, the less well-resolved structure is ascribed to double excitation and shape resonance. These assignments were made by using the "NO and NO^+ analogy" where the removal of a K-shell electron produces an NO-typecore [20].

Fig. 4 shows the photoion yield curve of N^+ in the 2.8-3.14 nm wavelengths (394.8-442.8 eV) region. Besides the sharp and intense $N(1s)\rightarrow 2p\pi_g$ transition, the N^+ ion exhibits low-intensity structures to shorter wavelength.

Between the N_K-edge and the $N(1s)\rightarrow 2p\pi_g$ transition, $N(1s)\rightarrow(nl)^1$ Rydberg orbital transitions are identified and converging to the $N(1s^{-1})$ ionization [18]. Position in energy, and assignments are gathered in table 2, together with the latest and most accurate previous measurements on N_2 by electron energy-loss spectroscopy [17]. The wavelength scale is calibrated by taking the high-resolution EELS values for the $N(1s)\rightarrow\pi^*$, υ=0 and υ=1 transitions at 3.094 nm (400.70 eV) and 3.092 nm (400.93 eV), respectively [17]. Both transitions being of about the same intensity, the center of the present $N(1s)\rightarrow\pi^*$ resonance is set at the average wavelength of 3.092 nm (400.82eV).

Fig. 2. *Normalized N^+/N_2 photoion yield curves as obtained for different retarding potential settings V_R. The retarding potential curve of N^+ observed at 2.959 nm (419 eV) in inserted for comparison.*

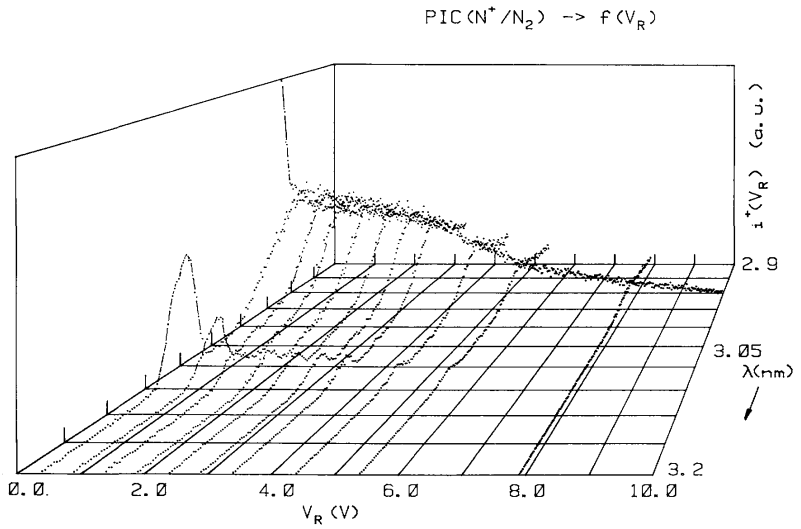

Published in: Chemical Physics (1992) vol. 160, pp. 477-485.
Status: Postprint (Author's Version)

Fig. 3. *Ion retarding potential difference (IRPD) curves obtained for different initial translational energies of N^+/N_2.*

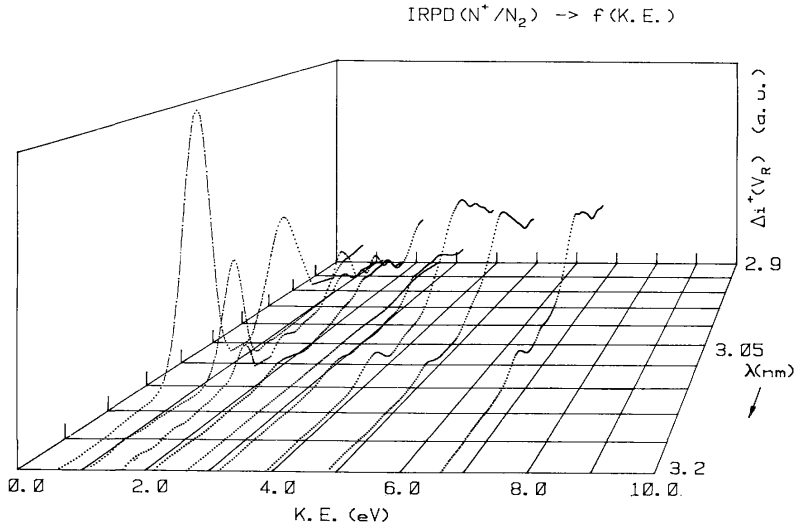

In the framework of the NO-analogy the N($1s^{-1}$) ionization onset has to be observed at 400.82+ 9.26=410.08 eV [24]. The ESCA value is 409.9 eV [25].

Assuming the sharp increase in the N^+ photoion yield at about 3.02 nm being due to $N_2^+(1s^{-1})$ formation, the measurement of its onset has been attempted. Fig. 4 shows the N^+ ionization efficiency curves at three different retarding potential settings. At V_R=8.0 V the N(1s)→2pπ_g resonance has almost disappeared. At higher energies, i.e. in the N(1s)→$(nl)^1$ region, a slight increase in the background precedes a fairly sharp increase of the N^+ photoion yield. By linear extrapolation (see fig. 4) an energy IE[$N_2(1s^{-1})$] = 3.019±0.004 nm (410.67±0.6 eV) is obtained, which has to be compared with the ESCA value 409.9 eV [25].

In the N^+ ionization efficiency curve, above the N $(1s)^{-1}$ level, more or less sharp and better resolved features are observed and their positions in energy are listed in table 2. The energy intervals of 6.57, 7.50 and 8.06 eV are measured above the first ionization energy. These energies correspond to those observed for $NO^+(a^3\Sigma)$ (6.40 eV), $NO^+(b^3\Pi)$ (7.30 eV) and $NO^+(b'^3\Sigma^-)$ (8.33 eV) [24]. On the basis of the close correlation between these data and the present measurements, the structures have to be assigned to the formation of [$N_2^+(1s^{-1})$]* states [18].

Table 2. *Wavelengths (nm), energies (eV), term values (eV) and assignments for the features observed in the N^+ photoionizationefficienc curve (see fig. 4): E(eV) = 1239.854/λ(nm). For the energy scale calibration, see text*

λ (±0.001)	*E*(±0.2)	*T*(±0.2)	Refs. [13,14,25]	Assignment
3.093	400.82	9.85	400.86	2pπ_g
3.083	402.14	-	vibr.	
3.078	402.83	-	struct.	
3.053	406.11	4.56	406.29	3sσ
3.046	407.10	3.57	407.18	3pπ, 3pσ_u
3.036	408.36	2.31	408.44	3dπ
3.025	409.81	0.86	409.12	5pπ, 6pπ
broad			409.9	
3.019 [a)]	410.67 [a)]	0[a)]	409.9 [b)]	N($1s^{-1}$)
± 0.004	± 0.6			
2.988	414.93	-4.26	414.0	
2.973	417.04	-6.57	415.0	[$N_2^+(1s^{-1})$]
2.965	418.17	-7.50	-	
2.961	418.73	-8.06	418.9	

[a)] Measured by the way described in text. [b)] ESCA N($1s^{-1}$) ionization energy.

Published in: Chemical Physics (1992) vol. 160, pp. 477-485.
Status: Postprint (Author's Version)

Fig. 4. *Photoionization efficiency curves of N^+/N_2 recorded at V_R= -0.5 V, 5.5 V and 8.0 V showing the steep decrease of the process at 3.095 nm (400.6 eV). The vertical bar locates the N (1s)$^{-1}$ ionization energy.*

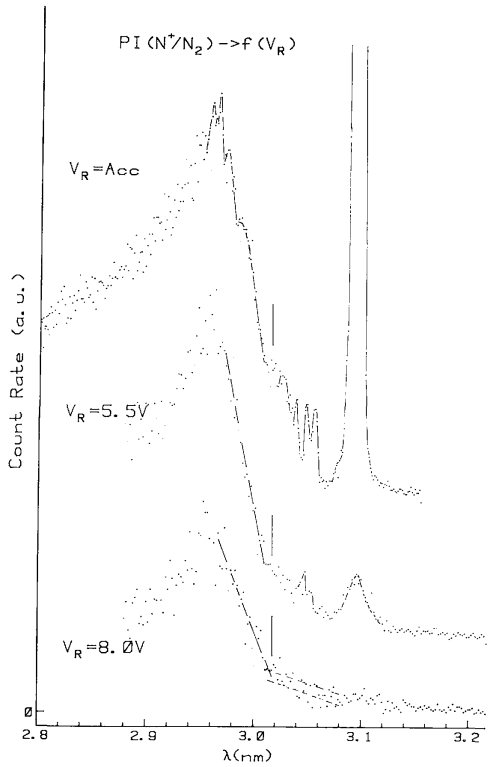

4.2. The N^+ photoion yield curves recorded at different retarding potential settings

The N^+ photoion yield curves recorded at different retarding potential settings (see fig. 2) and the resulting IRPD-curves (see fig. 3) have to be compared with the results of Saito and Suzuki [4-8] using electron-ion and ion-ion coincidence techniques. The IRPD-curves of N^+ are directly related to the N^+ ion yield curves measured for preset N^+ flighttimes [4].

As shown in fig. 3 the intensity of all processes shows strong variations upon the N^+ initial translational energy. However, the intensity of the N(1s)→π* resonance rapidly decreases and the IRPD-curves at N^+ translational energies above 2.6 eV are dominated by the high-energy process. Referring to fig. 4 in ref. [3], the present results are in good agreement with those obtained by Saito and Suzuki [4] over the whole photon energy range. Noteworthy is that for KE(N^+) = 2.1 eV, at high photon energies two distinct maxima at 2.9 nm (427 eV) and 2.97 nm (417 eV), respectively, are also observed in this work. The intensity increase at about 2.92 nm (424.6 eV) observed for KE(N^+) > 4.9 eV agrees with the observations of Saito and Suzuki [4].

The major discrepancy to be noticed is the relative intensity of the N(1s)→π* resonance to the shape resonance at 2.96 nm (418.8 eV). By the kinetic energy-selected N^+ ionization efficiency, the process at 3.095 nm (400.6 eV) steeply decreases for 0< KE(N^+)<2.0 eV as the shape resonance does. For higher N^+ translational energies, i.e. for KE(N^+) above 2.0 eV the latter process dominates. Referring to figs. 1, 2 and 4, at KE(N^+) = 8.0 eV, the intensity of the resonance peak at 3.095 nm (400.6 eV) does not emerge from the background. Contrarily, by the coincidence technique the N (1s) →π* resonance is the most intense process for 0<KE<10.3 eV [4]. This discrepancy cannot be explained by discrimination effects nor by a detection efficiency dependence on the initial translational energy of N^+. Discrimination is expected in the present experiment, the ion extraction field being about 120 mV/cm whereas in the work of Saito and Suzuki the ion acceleration was set at 130 V/cm [5]. These instrumental characteristics would almost influence the N^+ intensity ratio of low-to-high translational energy. However, N^+ fragments carrying the same kinetic energy should be detected with the same efficiency at 3.096 and at 2.96 nm. On the other hand, the N^+ anisotropic distribution has not to be taken into account, the N^+ fragments being detected in both experiments at right angles with respect to the photon beam.

Published in: Chemical Physics (1992) vol. 160, pp. 477-485.
Status: Postprint (Author's Version)

One reason for this discrepancy could be an underestimate of false coincidences at 3.09 nm [5]. Owing to the low intensity of the N^+ ion signal at high translational energies, it would become more sensitive to this correction.

On the other hand, the highest contribution to energetic N^+ ions could be expected from the Coulomb explosion through $N_2^{2+} \rightarrow N^+ + N^+$ or $N_2^{3+} \rightarrow N^{2+} + N^+$ which would have a larger contribution at 2.96 nm than at 3.09 nm. This fact is not expressed by the partial ion yield for different N^+ initial kinetic energies shown by Saito and Suzuki [4]. However, the same authors recorded the photon energy dependence of the PIPICO-signal related to the ion pairs $N^+ + N^+$ and $N^+ + N^{2+}$ [6]. In this work the π^*-resonance shows about 10% of the σ^*-resonance intensity for the former dissociation, whereas the π^*-resonance intensity falls in the background for the latter decomposition. The present photoionization data would corroborate these results.

4.3. The N^+ translational energy distributions

The N^+ translational energy distributions deduced from the IRPD-curves, as observed at 3.095 nm (400.6 eV), 3.05 nm (406.5 eV) and 2.959 nm (419.0 eV), respectively, are represented in fig. 5. Beside a high intensity and sharp thermal energy component, several distributions are observed with maxima near 1.5, 4.0 and at about 7 eV. However, at λ=3.095 nm (400.6 eV) only the two latter distributions are resolved. The low-energy component at about 1.5 eV could presumably be buried under the tail of the high-intensity thermal peak. On the other hand, at λ= 3.05 nm (404.8 eV) no thermal ion peak is observed.

Fig. 5. *Translational energy distributions of N^+/N_2 at λ=3.095 nm (400.6 eV), 3.05 nm (406.5 nm) and 2.959 nm (419 eV) obtained from the IRPD-curves.*

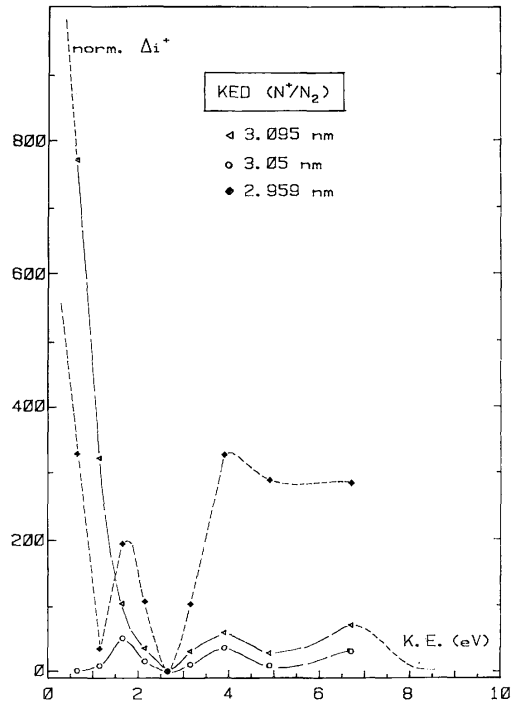

The present data are compared to the kinetic energy spectra obtained by Yagishita et al. [26] by using a parallel-plate analyzer without mass discrimination. These measurements were performed at 0° and 90° with respect to the polarization direction of the photon beam. At the N(1s)→π^* resonance and under 90°, the distribution shows a strong thermal component and a weak distribution peaking at 5.6 eV. At the σ^* shape resonance the distribution is made of three components, i.e. at thermal energy, at about 1.5 eV and 5.5 eV. At both 3.095 nm (401 eV) and 2.959 nm (419 eV) the distribution extends to about 10 eV translational energy.

These distributions have to be compared with the results obtained by Saito and Suzuki [5,6,8]. At λ=2.959 nm (419 eV) the translational energy spectrum of N^+ shows a weak maximum near 1.5 eV, a fairly broad and intense distribution with a maximum at about 4.5 eV and a long tail extending to up to 16 eV. The

intensity ratio $i(N^+)_{1.5eV}/\ i(N^+)_{4.5ev}$= 1/3. In the present work the same ratio is 4/5. For translational energies above 4 eV the present results can be compared with the ion-ion (N^++N^+) coincidence work [6].

The thermal component detected in the present work is more intense than in the work of Saito and Suzuki [4]. Compared to the numerically first differentiated retarding curve of N_2^+ at λ=3.095 nm (400.6 eV) the thermal peak at λ=2.959 nm (419 eV) is significantly narrower, corroborating the TOF-mea-surements [5,8]. This zero kinetic energy peak is exclusively assigned to N_2^{2+} ions [5]. However, as mentioned earlier in this section, at this wavelength low translational energy N^+ ions probably contribute to the high-energy tail of the thermal peak.

The numerous possible pathways for neutral-ion (N+N^+ and N+N^{2+}) and ion-ion (N^++N^+ and N^++N^{2+}) dissociations were extensively discussed by Eberhardt et al. [2,3] and Suzuki and Saito [4-8]. Essentially, three photon energy ranges have to be considered.

At the π*-resonance, after Auger decay, essentially the configurations $V^{-2}1\pi_g$ or $2\sigma^{-1}V^{-1}1\pi_g$ (where V represents a valence orbital) dissociate into N^+ +N or N^+ +N^+ where N^+ should carry 0.2-4.4 eV trans-lational energy. For higher kinetic energies two hole states of N_2 would be involved, e.g. V^{-2} or $2\sigma^{-1}V^{-1}$ [4,5].

At the Rydberg excitations the resulting Rydberg states deexcite to, e.g. V^{-1} (*nl*) or $2\sigma_gV^{-1}$(*nl*) (where *nl* represents a Rydberg orbital) which autoionize and dissociate into N^+ + N, N^+ or N^{2+} [8].

Finally, at the σ*-resonance V^{-2} and $2\sigma^{-1}V^{-1}$ states are produced by Auger transitions and N^+ +N^+ and N^++N^{2+} dissociations have been proposed [4,5].

Without mass selection, Yagishita et al. [26] observed a kinetic energy distribution peaking at 1.5 eV for 2.95 nm (419 eV) photons. They ascribed it to the N_2^{2+} (≈60 eV)→N^++N (at 54 eV). For mass selected N^+ ions this distribution is also observed by Suzuki and Saito [5] and in the present work. On the other hand, Suzuki and Saito [5] do not measure a low kinetic energy N^{2+} component at 2.95 nm (419 eV). This would probably mean that the transla-tional energy distribution observed at 1.5 eV could be ascribed to N_2^{2+} (V^{-2} at ≈44 eV)→N^++N^+ + 3 eV (≈41 eV) at 2.95 nm (419 eV) photon energy. The same distribution is observed at 3.05 nm (406 eV) and the dissociative autoionization $N_2[(1s\text{-}^1)\ (nl)]$→$N_2^{2+}$ (V^{-2} at ≈44 eV)→N^+ +N^+ + 3 eV (≈41 eV) could be involved.

5. Conclusion

The N_2^+ and N^+ ion formation from N_2 has been investigated at medium resolution by photoionization mass spectrometry in the inner-shell excitation and ionization energy region (2.8-3.2 nm). A retarding potential is used to analyze (i) the translational energy of the N^+ fragment ions at fixed wavelength and (ii) the ionization efficiency at fixed retarding potential settings.

Beside the direct $N(1s)^{-1}$ onset determination from the present data, several sharp features at 6.6, 7.5 and 8.1 eV above the $N(1s)^{-1}$ threshold were identified in the N^+ ion yield curve and assigned to $[N_2^+(1s)^{-1}]$* excited states.

The main goal of this work was to apply the ion retarding potential difference (IRPD) method [9] to resonance phenomena to obtain translational energy distributions at several wavelengths. In the case of N^+/N_2 the dissociative ionization in the inner-shell ionization energy region has been extensively investigated [2-8]. The comparison between the present results and those obtained by TOF-measurements is quite satisfactory. This would allow us to apply the same method to other molecular systems.

Acknowledgement

We wish to thank the Belgian Fonds de la Recherche Scientifique (FNRS) and the Bundesminis-terium fur Forschung und Technologie (BMFT) for financial support. We are indebted to H.W. Jochims for his valuable assistance. One of us (RL) acknowledges the European Community for a contract [GE1-0018-D(B)] within its LSI-program.

Published in: Chemical Physics (1992) vol. 160, pp. 477-485.
Status: Postprint (Author's Version)

References

[1] D.M. Hanson, Advan. Chem. Phys., Vol. 77, eds. I. Prigogine and S.A. Rice (Wiley/Interscience, New York, 1990) p. 1.

[2] W. Eberhardt, J. Stohr, J. Feldhaus, E.W. Plummer and F. Sette, Phys. Rev. Letters 51 (1983) 2370.

[3] W. Eberhardt, E.W. Plummer, I.W. Lyo, R. Carr and W.K. Ford, Phys. Rev. Letters 58 (1987) 207.

[4] N. Saito and I.H. Suzuki, Chem. Phys. Letters 129 (1986) 419.

[5] N. Saito and I.H. Suzuki, Intern. J. Mass Spectrom. Ion Processes 82 (1988) 61.

[6] N. Saito and I.H. Suzuki, J. Phys. B 20 (1987) L785.

[7] N. Saito and I.H. Suzuki, J. Phys. B 22 (1989) 3973.

[8] I.H. Suzuki and N. Saito, J. Chem. Phys. 91 (1989) 5324.

[9] R. Locht, G. Hagenow, K. Hottmann and H. Baumgärtel, Chem. Phys. 151 (1991) 137.

[10] R.A. Rosenberg, P.J. Love, P.R. LaRoe, V. Rehn and C.C. Parks, Phys. Rev. B 31 (1985) 2634.

[11] R. Locht, J. Momigny, E. Rühl and H. Baumgärtel, Chem. Phys. 117 (1987) 305.

[12] S. Bernstorff, W. Braun, M. Mast, W. Peatman and T. Schroeter, Rev. Sci. Instrum. 60 (1989) 2097.

[13] R. Locht and J. Schopman, Intern. J. Mass Spectrom. Ion Phys. 15 (1974) 361.

[14] K. Köllmann, Intern. J. Mass Spectrom. Ion Phys. 17 (1975) 261.

[15] J.A.D. Stockdale and L. Deleanu, Chem. Phys. Letters 22 (1973) 204.

[16] G.R. Wight, CE. Brion and M.J. van der Wiel, J. Electron. Spectry. Relat. Phenom. 1 (1972/73) 457.

[17] A.P. Hitchcock and C.E. Brion, J. Electron. Spectry. Relat. Phenom. 18 (1980) 1.

[18] M. Tronc, G.C. King and F.H. Read, J. Phys. B 13 (1980) 999.

[19] D.A. Shaw, G.C. King, F.H. Read and D. Cvejanovic, J. Phys. B 15 (1982) 1785.

[20] M. Nakamura, M. Sasanuma, S. Sato, M. Watanabe, H. Yamashita, Y. Igushi, A. Ejiri, S. Nakai, S. Yamaguchi, T. Sagawa, Y. Nakai and T. Oshio, Phys. Rev. 178 (1969) 80.

[21] A. Bianconi, H. Petersen, F.C. Brown and R.Z. Bachrach, Phys. Rev. A17 (1978) 1907.

[22] M. Domcke, A. Puschmann, T. Mandel and G. Kaindl, Annu. Report BESSY (1989) 340.

[23] B. Locht, W. Denzer, H.W. Jochims and H. Baumgärtel, unpublished results.

[24] O. Edqvist, L. Åsbrink and E. Lindholm, Z. Naturforsch. 26a (1971) 1407.

[25] K. Siegbahn, C. Nordling, G. Johansson, J. Hedman, P.F. Heden, K. Hamrin, U. Gelius, T. Bergmark, L.O. Werme, R. Manne and Y. Baer, ESCA Applied to Free Molecules (North-Holland, Amsterdam, 1969).

[26] A. Yagishita, H. Maezawa, M. Ukai and E. Shigemasa, Phys. Rev. Letters 62 (1989)36.